Using Solar Wind Helium to Probe the Structure and Seasonal Variability of the Martian Hydrogen Corona

J. S. Halekas[1], J. P. McFadden[2]

[1]Department of Physics and Astronomy, University of Iowa, Iowa City, IA 52242 USA.

[2]Space Sciences Laboratory, University of California, Berkeley, CA 94720 USA.

Corresponding author: Jasper S Halekas (jasper-halekas@uiowa.edu)

Key Points:

- Singly ionized helium is produced upstream from Mars by charge exchange between solar wind alpha particles and Martian neutral hydrogen
- The observed ratio of singly to doubly ionized helium varies as expected with solar wind speed, spatial location, and Martian season
- Helium ion measurements can be utilized to estimate the column density of hydrogen in the Martian corona and its seasonal variability

Abstract

We utilize measurements from instruments on the Mars Atmosphere and Volatile EvolutioN (MAVEN) mission to investigate singly ionized helium formed by charge exchange between solar wind alpha particles and neutral hydrogen in the region upstream from Mars. We show that the observed helium ion signal varies with solar wind speed and spatial location in a manner consistent with expectations for a charge exchange source. We find that the ratio of singly to doubly ionized helium varies with Martian season, with a peak in the southern summer season. The inferred neutral hydrogen column density and the seasonal variation thereof agree with the results of previous studies based on other measurement techniques. The MAVEN helium ion measurements provide a new method of probing the hydrogen corona, with nearly continuous coverage of the Martian seasonal cycle across the entire mission, enabling study of the interannual variability of the Martian exosphere.

Plain Language Summary

Thanks to Mars' small size and weak gravity, the upper reaches of its atmosphere extend far above the surface. The lightest element, hydrogen, forms a corona around Mars many times larger than the planet. The solar wind that flows from the Sun, composed mainly of protons and alpha particles (doubly ionized helium), interacts directly with this hydrogen corona. Reactions between solar wind alpha particles and neutral hydrogen in the corona can form singly ionized helium. We utilize measurements from instruments on the Mars Atmosphere and Volatile EvolutioN (MAVEN) mission to investigate the singly ionized helium signature in the region upstream from Mars. We show that the measured signal varies with solar wind speed and distance from Mars as expected, and utilize it to probe the structure and seasonal variability of the Martian hydrogen corona. These measurements will ultimately allow us to better understand the Martian seasonal cycle and its role in the escape of hydrogen from the Martian atmosphere.

1 Introduction

The solar wind that flows outward from the Sun through our solar system is primarily composed of ionized hydrogen (protons, ~95% of the solar wind number density on average), but also contains doubly ionized helium (alpha particles, ~4%), and an admixture of other heavier ions (~1%), many multiply charged (Bame et al., 1968; Ogilvie & Coplan, 1995). The relative abundance of alpha particles in the solar wind ranges from <1% to ~10%, and varies with solar cycle, heliographic latitude, and solar wind speed (Aellig et al., 2001; Kasper et al., 2007).

In addition to doubly ionized helium (He^{++}), the solar wind sometimes contains a small amount of singly ionized helium (He^{+}). This can occur in unusually cold solar plasma (Gosling et al., 1980; Schwenn et al., 1980) such as that sometimes found in coronal mass ejections. He^{+} can also originate from ionization and pickup of interstellar neutral helium (Möbius et al., 1985), which produces a localized signature in the portion of the heliosphere downstream from the interstellar neutral flow, enhanced by the solar gravitational focusing of helium atom trajectories (Gloeckler et al., 2004).

The production of He^{+} can also occur in situ, by charge exchange between solar wind He^{++} and neutral gases. For example, charge exchange with volatiles in a cometary coma leads to

a ratio of singly to doubly ionized helium that increases with decreasing distance to the nucleus, with observations of this ratio thereby enabling reconstruction of the neutral density profile (Burch et al., 2015; Fuselier et al., 1991; Shelley et al., 1987; Wedlund et al., 2016).

Similar processes also occur at Mars, where charge exchange between the solar wind and neutrals in the Martian corona can remove up to 30% of the incident alpha particles, leading to deposition of solar wind helium in the Martian atmosphere (Chanteur et al., 2009; Stenberg et al., 2011). Helium, of exogenic and endogenic origin, also escapes from the Martian atmosphere, by both thermal and nonthermal processes (Barabash et al., 1995; Krasnopolsky et al., 1993).

A number of lines of evidence, including scattered Lyman-α (Bhattacharyya et al., 2015; Chaffin et al., 2014; Clarke et al., 2014), hydrogen pickup ions (Rahmati et al., 2018; Yamauchi et al., 2015), low frequency plasma waves driven by hydrogen pickup ions (Bertucci et al., 2013; J. S. Halekas et al., 2020; Romanelli et al., 2016; Romeo et al., 2021), and byproducts of charge exchange between solar wind protons and neutral hydrogen (J. S. Halekas, 2017) have demonstrated that the Martian hydrogen corona has a strong seasonal variability, peaking shortly after perihelion in the southern summer season. This seasonal variability apparently results from the Martian dust storm cycle, which enables transport of water to higher altitudes, where it undergoes destructive reactions that produce hydrogen that can then escape thermally (Chaffin et al., 2017; Fedorova et al., 2020; Stone et al., 2020).

The extended nature of the hydrogen corona exposes it directly to solar wind ions in the upstream region and Martian magnetosheath, enabling charge exchange between neutral hydrogen atoms and solar wind protons and alpha particles. In this manuscript, we exploit these characteristics and utilize the ratio of singly to doubly ionized helium to probe the structure and seasonal variability of the Martian hydrogen corona.

2 Helium Ion Measurements

We utilize measurements from the SupraThermal and Thermal Ion Composition (STATIC) and Solar Wind Ion Analyzer (SWIA) instruments on the Mars Atmosphere and Volatile EvolutioN spacecraft (J. S. Halekas et al., 2015; Jakosky et al., 2015; McFadden et al., 2015) to characterize the incident solar wind and measure the relative abundance of singly and doubly ionized helium around Mars. We utilize a combination of direct observations of the solar wind by SWIA in the upstream region and proxy data based on SWIA measurements of precipitating hydrogen in the upper atmosphere to characterize the solar wind speed (J. S. Halekas et al., 2017), which determines the charge exchange cross section between solar wind He^{++} and neutral hydrogen (Barnett et al., 1990). We utilize STATIC measurements to determine the ion energy per charge and mass per charge around Mars. We primarily employ the STATIC *c6* product, which retains the best combined energy and mass resolution (32 energies x 64 masses), but sums over all look directions.

Figures 1 and 2 demonstrate our analysis methods. For all STATIC measurements, we utilize a basic background subtraction that removes the signature of proton and alpha particle straggling that can lead to spurious counts at the same energy per charge but in other mass per charge ranges (McFadden et al., 2015). We then separate the STATIC measurements into mass per charge bins, using mass per charge ranges of 0.7-1.4 to characterize protons, 1.4-2.5 to characterize He^{++}, and 2.8-5.0 to characterize He^{+}. These broad mass per charge bins account for

variations in time of flight in the sensor as well as the accuracy of timing and binning counts into mass tables onboard. These mass per charge bins can also contain other ions, notably including molecular hydrogen ions (primarily of magnetospheric origin) in the He^{++} bin and other heavier multiply charged ions (primarily of solar wind origin) in both helium ion bins.

We next filter by energy per charge, in order to focus on ions approximately co-moving with the solar wind protons. We compute the characteristic energy of the protons $\langle E_p \rangle = \int E_p f_p(v) d^3v / \int f_p(v) d^3v$ as a first estimate of the energy of the solar wind flow. For cases where this value is lower than the energy of the peak proton differential energy flux, we take the latter as a better estimate of the solar wind energy, in order to mitigate against the presence of low energy populations that skew the characteristic energy estimate. We then select ions in the He^{++} mass per charge range with energies per charge from 1.5 to 3.5 times that of the solar wind, and ions in the He^{+} mass per charge range with energies per charge from 3.0 to 7.0 times that of the solar wind. For He^{+}, we also track a narrower mass per charge range of 3.3-4.4, and a narrower energy per charge range of 2.8 to 5.0 times the proton characteristic energy (as shown in Fig. 2), in order to determine whether the energy-mass distribution has a local maximum in the He^{+} bin.

The top three panels of Fig. 1 show energy-time spectra for ions in the three mass per charge ranges, with the selected energy per charge ranges indicated. Fig. 2 shows a full energy-mass distribution, with the selected mass per charge and energy per charge ranges marked. We find clear peaks in differential energy flux in the selected mass per charge and energy per charge ranges, but also note the presence of some weaker fluxes outside of these ranges. In the proton mass per charge range, we observe non-negligible fluxes both above and below the main solar wind peak. The lower energy protons primarily result from scattering of the solar wind from spacecraft and instrument surface, while the higher energy protons most likely represent hydrogen pickup ions and/or solar wind protons reflected at the bow shock or in the magnetosheath. We also note the presence of other ions roughly co-moving with the solar wind (which appear along the same diagonal arc in the energy-mass distribution), likely consisting of an admixture of heavier multiply charged solar wind ions. Finally, we observe a weak signal in the He^{+} mass per charge range at a higher energy per charge than expected for ions co-moving with the protons, which may indicate the presence of reflected and/or pickup helium ions.

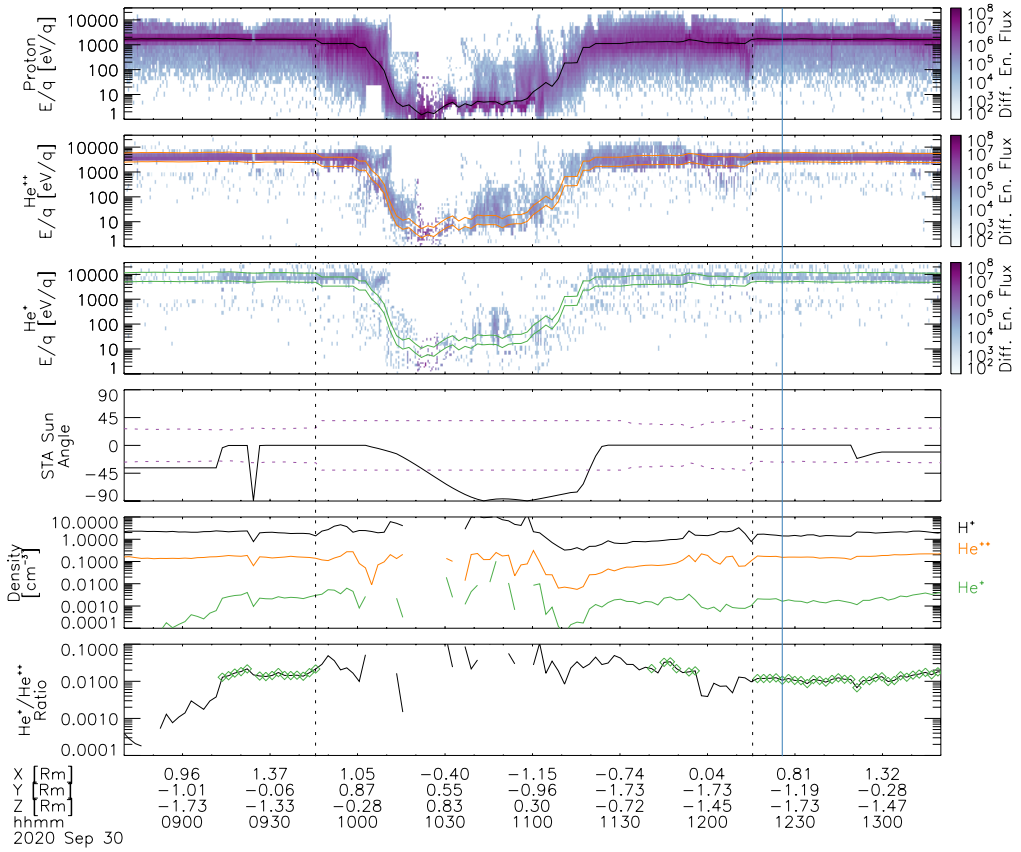

Figure 1. Measurements made by the SupraThermal and Thermal Ion Composition (STATIC) instrument on the Mars Atmosphere and Volatile EvolutioN (MAVEN) spacecraft on 30 September 2020. The top three panels show energy per charge spectra for ions with mass per charge consistent with protons, doubly ionized helium (He^{++}), and singly ionized helium (He^{+}), in units of differential energy flux (eV/[cm^2 s sr eV]). The black line in the first panel shows the proton characteristic energy, and the orange and green lines in the second and third panels bracket the expected energy ranges for helium ions co-moving with the protons. The fourth panel shows the angle between the sunward vector and the undeflected STATIC field of view (solid), as compared to the maximum deflection angles for which STATIC can measure singly ionized helium with the solar wind speed (dashed). The fifth and sixth panels show the densities for ions in the three mass per charge ranges and the solar wind speed range, and the ratio between the singly and doubly ionized helium densities. Green diamonds in the bottom panel indicate points that meet all selection criteria described in the text. Labels at the bottom of the plot indicate the time and the location of the measurement in Mars-Solar-Orbital coordinates (in units of Mars radii). The vertical black dashed lines indicate the bow shock location, and the vertical blue line indicates the time of the measurement shown in Fig. 2.

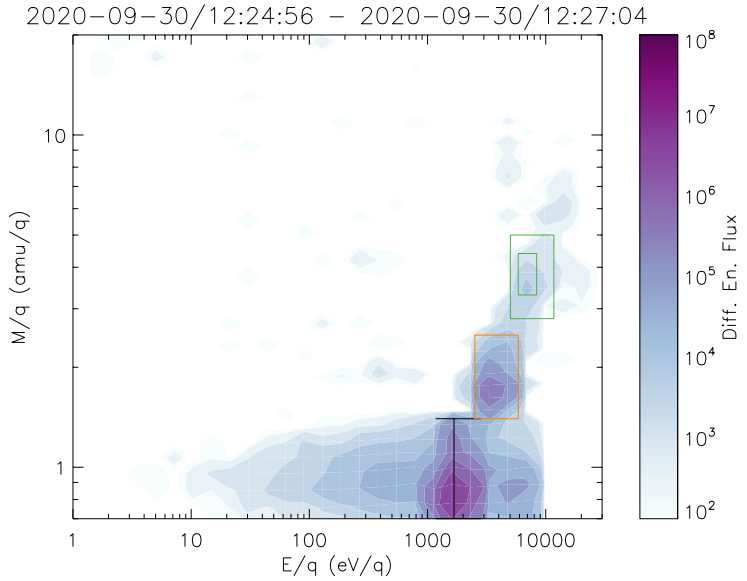

Figure 2. Sample energy-mass distribution measured by STATIC, accumulated over a 128 s time range, in units of differential energy flux (eV/[cm^2 s sr eV]). The black lines show the mass per charge range utilized to compute proton density, and the proton characteristic energy. The orange box shows the mass per charge and energy per charge range utilized to compute He^{++} density. The outer green box shows the mass per charge and energy per charge range utilized to compute He^{+} density, and the inner green box shows the ranges utilized to characterize the peak of the He^{+} distribution (see text).

Using the mass per charge and energy per charge ranges defined above, we compute estimates of the densities of protons and doubly and singly ionized helium, as well as the ratio of singly to doubly ionized helium densities, as shown in Fig. 1. To improve statistics, we accumulate over 128 s intervals, co-adding all STATIC *c6* products within each interval (nominally 32 individual 4-s accumulations), before background-subtracting and computing partial density moments.

STATIC relies on electrostatic deflectors to cover its field of view (FOV), which has an azimuthal angle (anode angle) range of 360° and a maximum polar angle (deflection angle) range of ±45°. The constrained range of the high voltage that controls the electrostatic deflectors results in a reduced deflection angle range at higher energies. Since we primarily focus on solar wind ions, we track the angle between the sunward direction and the undeflected FOV, and compare to the maximum angular range over which STATIC can detect He^{+} with four times the energy per charge of the protons, as shown in Fig. 1. When the sunward direction falls outside of this angular range, the He^{+} signal typically drops significantly, as seen in the early portion of the orbit of Fig. 1. We therefore require that the sunward direction lies within the accessible FOV for the He^{+} energy per charge range, maximizing the likelihood that we can detect the signal of interest.

We also apply a number of other selection criteria to the densities and density ratios that we derive. We require that the average differential energy flux in the inner mass per charge and energy per charge range for He^{+} exceeds the average over the entire He^{+} bin by at least 25%, to

eliminate cases where ions with other energies and/or masses dominate over the desired signal. We also require an He^{++} density greater than 0.04 cm^{-3}, and a relative He^{++} to proton density ratio between 0.01 and 0.12, in order to ensure adequate statistics and rule out physically implausible solar wind conditions. Finally, we restrict our analysis to observations with proton characteristic energies greater than 500 eV, in order to focus on the solar wind and magnetosheath, and to eliminate data taken in off-nominal operating modes. The green diamonds in Fig. 1 indicate the observations that meet all of these selection criteria, for this time range.

We carry out the analysis described above for the entire MAVEN science mission, and show the results in Figure 3. We find a high degree of variability in the individual measurements, likely resulting from a combination of statistical fluctuations, solar wind variability, differing observation geometries, and multiple populations of ions. Nonetheless, we do observe a clear and reproducible signature of seasonal variability in the observed He^{+} densities, both in the raw measurements, and more clearly in the median values.

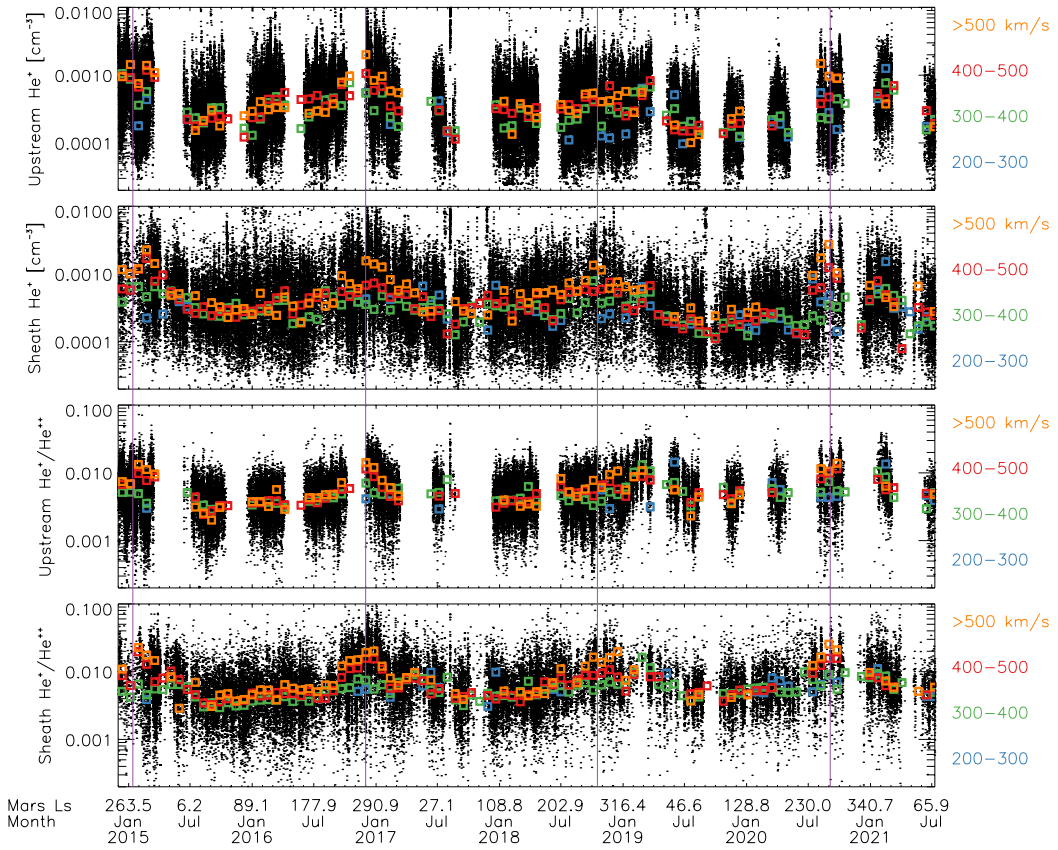

Figure 3. Helium ion densities measured by STATIC over the entire MAVEN mission. The four panels show He^{+} densities from locations outside of the nominal bow shock (upstream) and between the nominal magnetic pileup boundary and bow shock (sheath), and ratios between singly and doubly ionized helium densities for the same regions. The black dots show individual 128 s accumulations meeting all selection criteria described in the text. The colored squares show 24-day medians for four ranges of solar wind speed measured by the Solar Wind Ion Analyzer (SWIA). The vertical purple lines indicate Mars solar longitudes (L_S) of 270° (southern summer solstice).

The observed He^+ densities clearly peak in the southern summer season, at a Mars solar longitude (L_S) of ~270°, consistent with the known variability of the Martian hydrogen corona (Bertucci et al., 2013; Bhattacharyya et al., 2015; Chaffin et al., 2014; Clarke et al., 2014; J. S. Halekas, 2017; Rahmati et al., 2018; Romanelli et al., 2016; Romeo et al., 2021). Dividing the measured He^+ density by the He^{++} density reduces the observed level of variability considerably and more clearly reveals the seasonal trends, as one would expect, since this normalization accounts for the variation in solar wind composition from stream to stream and thereby reduces the confounding effects of changing solar wind conditions.

We utilize conic section models of the Martian bow shock and magnetic pileup boundary (Trotignon et al., 2006) to separate the observations into regions upstream of the nominal bow shock location and between the nominal bow shock and magnetic pileup boundary locations (i.e. in the magnetosheath). We find a greater median He^+ abundance in the magnetosheath than in the solar wind, as expected for products of charge exchange, since ions in the sheath have traveled through a greater column density of neutral hydrogen. We also observe a larger He^+ signal for higher solar wind speeds, again consistent with a charge exchange origin, given the steep increase in the $He^{++} + H \rightarrow He^+ + H^+$ charge exchange cross section with He^{++} energy (Barnett et al., 1990).

3 Solar Wind Variability

We further investigate the speed dependence of the observed He^+ signal by plotting the data in Fig. 3 as a function of speed for a series of L_S bins, as shown in Fig. 4. In the upstream region, we find a nearly constant apparent ratio of singly to doubly ionized helium, on the order of ~0.004, for most L_S ranges. However, in the southern summer 240-300° L_S range, we observe a density ratio that increases with solar wind speed. Assuming no background and production solely by charge exchange between alpha particles and neutral hydrogen, the observed speed dependence of the upstream signal in the 240-300° L_S range would imply a median hydrogen column density of ~2.2×10^{13} cm^{-2}. On the other hand, if we subtract a constant background ratio of 0.004, as suggested by the observations, the observed speed dependence of the upstream signal implies a hydrogen column density of ~1.6×10^{13} cm^{-2}. The observed speed dependence of the helium ion density ratio closely agrees with that expected based upon measured charge exchange cross sections (Barnett et al., 1990), particularly with the addition of an assumed steady-state background level.

For observations in the sheath, we again find a roughly constant ratio of ~0.004 in the 0-60°, 60-120°, and 120-180° L_S ranges (the three ranges surrounding aphelion at L_S of 71°). We observe a small signal, with a slight apparent increasing trend with solar wind speed, in both the 180-240° and 300-360° L_S ranges, and a much more prominent signal with a clear solar wind speed dependence in the 240-300° L_S range. Assuming no background and production solely by charge exchange between alpha particles and neutral hydrogen, the observed speed dependence of the magnetosheath signal in the 240-300° L_S range would imply a median hydrogen column density of ~3.3×10^{13} cm^{-2}. Meanwhile, assuming the same constant background ratio of 0.004 as above, the observed speed dependence of the magnetosheath signal implies a hydrogen column density of ~2.8×10^{13} cm^{-2}. This range of values of column density agrees well with previous

inferences based on charge exchange between solar wind protons and Martian neutral hydrogen upstream of the bow shock for this L_S range (J. S. Halekas et al., 2017).

The origin of the apparent steady-state background level of ~0.004 remains uncertain. Given the lack of a clear seasonal dependence, it most likely does not result from processes that would vary with orbital position, such as pickup of interstellar helium. Given the lack of a clear difference between the apparent background level in the upstream and magnetosheath regions, it most likely does not result from charge exchange with other Martian exospheric neutral species (such as oxygen) that do not have strong seasonal variations (Rahmati et al., 2018). Therefore, the admixture of other solar wind minor ion species in the observations and/or the presence of additional instrumental backgrounds not accounted for in the analysis provide the most likely explanations for the observed systematics.

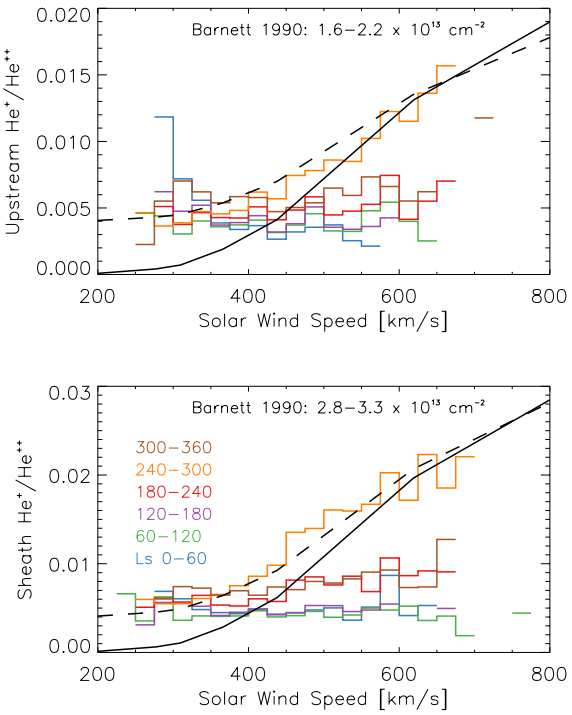

Figure 4. Helium ion density ratios measured by STATIC over the entire MAVEN mission, from locations outside of the nominal bow shock (upstream) and between the nominal magnetic pileup boundary and bow shock (sheath), with median ion density ratios as a function of solar wind speed for six L_S ranges. Black lines show expected ion density ratios given measured cross sections for charge exchange between He^{++} and neutral hydrogen (Barnett et al., 1990) and inferred neutral hydrogen column densities for the southern summer solstice L_S range, assuming no background (solid lines, upper range of column densities), and a constant background level of 0.004 (dashed lines, lower range of column densities).

4 Seasonal Variability

Given the speed dependence of the relevant charge exchange cross section, the measurements made during conditions with high solar wind speed provide the clearest record of

the seasonal variability of the Martian hydrogen exosphere. We therefore proceed to analyze the helium ion measurements obtained during times with solar wind speeds greater than 500 km/s to investigate the seasonal variability, as shown in Fig. 5. We find ratios of singly to doubly ionized helium ranging from ~0.004 to 0.02, with a peak at L_S of ~270-300°, and generally higher values in the sheath region than in the upstream region.

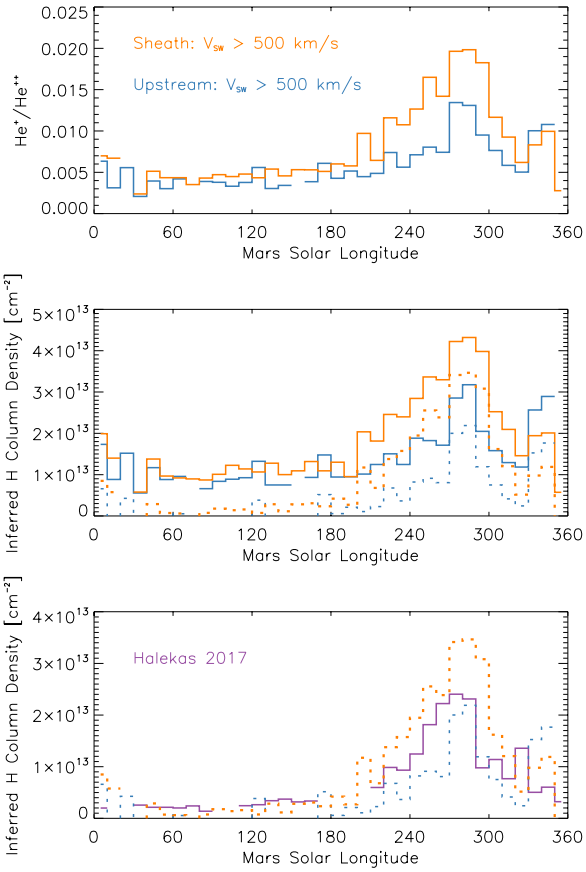

Figure 5. Helium ion density ratios measured by STATIC over the entire MAVEN mission, for the highest solar wind speed range (> 500 km/s), as a function of Mars solar longitude. The top panel shows median helium ion density ratios for measurements made outside of the nominal bow shock (upstream) and between the nominal magnetic pileup boundary and bow shock (sheath). The middle panel shows median inferred neutral hydrogen column densities, with (dashed lines) and without (solid lines) subtraction of a constant background helium ion density ratio of 0.004. The bottom panel shows the same hydrogen column density estimates derived from helium ions (dashed lines, with background subtraction), together with a previous estimate (purple lines) derived from byproducts of charge exchange between solar wind protons and Martian hydrogen (J. S. Halekas, 2017).

We can convert the observed helium ion density ratios to column density estimates, using the same charge cross sections employed above (Barnett et al., 1990). For all measurements made during times with solar wind speeds greater than 500 km/s, we convert the observed density ratios to inferred column densities, utilizing cross sections appropriate for the solar wind

speed corresponding to each individual measurement. We perform this same calculation with and without first subtracting an assumed constant background ion density level of 0.004, and show the resulting median estimated column densities in Fig. 5. The median column densities thereby estimated reproduce all the same trends as the raw helium ion density ratios, though they do not represent an exact multiple thereof, given minor statistical differences in the observed solar wind speed distributions in each L_S bin.

Taking the background-subtracted version of the inferred column densities as our best estimate for both the upstream and magnetosheath datasets, we compare to column density estimates based on charge exchange between solar wind protons and Martian neutral hydrogen (J. S. Halekas, 2017), as shown in Fig. 5. We find that the previous proton-based estimates generally lie directly between the column density values inferred from our upstream and magnetosheath helium measurements. Given that the proton-based measurements were processed to isolate the signal of the hydrogen column extending upstream from the bow shock, one would expect exactly this ordering of the observations, since the column density encountered at the bow shock lies between the median column density encountered in the upstream region and that in the magnetosheath region. This agreement appears quite encouraging, given that we used no adjustable or assumed parameters in either analysis, other than an assumed constant helium ion density ratio background level, which we based directly on the systematics of our observations. The proton-based data, though also covering a full range of seasons, only overlaps with the first half of the full time range covered by the helium ion dataset, so this level of agreement may also indicate a fairly consistent seasonal cycle.

We do note some level of disagreement in the L_S range 330-360°, with the helium ion extrapolations for both the upstream and magnetosheath regions exceeding the proton-based estimate. Intriguingly, this Ls range corresponds with the time period where Mars crosses the helium focusing cone. Previous measurements indicate a cone centered at an ecliptic longitude of ~74° (Gloeckler et al., 2004), which corresponds to an L_S of ~349° at Mars. At the orbit of Mars (similar to at 1 AU), the helium focusing cone should contain neutral helium with a density enhanced by a factor of ~5 over the crosswind direction, and an eliptic longitude extent on the order of ~30-40° FWHM (Gloeckler et al., 2004). This appears quite consistent with the morphology of the peak we observe in our data in this Ls range, suggesting that this feature may result at least in part from the pickup of interstellar helium. Previous measurements indicate peak He^+ differential energy fluxes for interstellar pickup ions on the order of ~10^4 eV/[cm^2 s sr eV] at 1 AU (Möbius et al., 1985). As Figs. 1 and 2 demonstrate, STATIC has the capability to detect such fluxes, at a level comparable to those arising from charge exchange with the Martian corona. Not all such pickup He^+ ions would have energies per charge in the band we selected for analysis, but a portion would, lending credence to this hypothesis for the origin of the features observed in this L_S range.

5 Spatial Variability

As a final consistency check, we investigate the spatial dependence of the observed helium ion density ratios around Mars. In order to best isolate the signal of interest, we focus on the southern summer L_S range of 240-300° and the highest solar wind speed range (>500 km/s), We convert the measured helium ion density ratios to estimates of the neutral hydrogen column density, utilizing the same analysis procedure and same nominal background subtraction as

above. We show the results in Figure 6, in cylindrical Mars-Solar-Orbital (MSO) coordinates. We find that the inferred column densities increase steadily from the upstream region to the inner magnetosheath, as expected for a source derived from charge exchange between the solar wind and the hydrogen corona. The lack of any discontinuities in the inferred column densities at the bow shock suggests that our analysis methods work reasonably well to select reliable helium ion observations in both the upstream and magnetosheath regions.

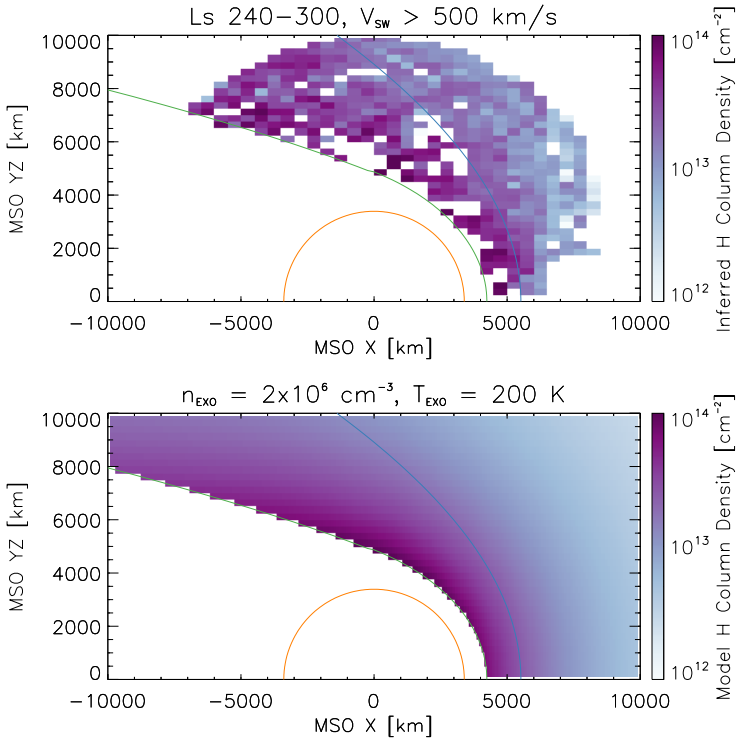

Figure 6. Inferred neutral hydrogen column densities derived from STATIC helium ion measurements (with background subtraction) for the southern summer solstice L_S range and the highest solar wind speed range (>500 km/s), as a function of location, in Mars-Solar-Orbital (MSO) coordinates. For comparison, the bottom panel shows hydrogen column densities computed from a Chamberlain exospheric model (Chamberlain, 1963) for a plausible exobase density of 2x10^6 cm^{-3} and temperature of 200 K, utilizing straight-line integrations along tangents parallel to the MSO *x* axis. The green and blue lines show the nominal positions of the magnetic pileup boundary and bow shock (Trotignon et al., 2006).

To provide an illustrative comparison, we utilize a Chamberlain exospheric model (Chamberlain, 1963) to compute a plausible neutral hydrogen density profile for an exobase density and temperature appropriate for this season, as determined from a previous analysis based on solar wind proton charge exchange (J. S. Halekas, 2017). We include no populated satellite orbits, as generally assumed. We calculate the corresponding column densities, using line-of-sight integrations along rays parallel to the Mars-Sun line (the MSO *x* axis). The solar wind ions do in fact follow approximately anti-sunward streamlines in the upstream region (neglecting the small aberration due to Mars' orbital motion), but have more curved trajectories in the magnetosheath, since the plasma flows deflect around the magnetic pileup boundary and

the magnetosphere. Therefore, we cannot straightforwardly compare the model column densities in the sheath to those derived from the helium ion density ratio. Nonetheless, even with the simplifying assumptions we utilized, the reasonable agreement between the inferred and model hydrogen column densities provides a useful consistency check.

In general, we expect the solar wind helium ions in the sheath to have encountered a somewhat larger column density than if they had followed straight-line anti-sunward paths. However, one would need to utilize a global model of the ion flow and compute the column density along ion streamlines to perform a more rigorous analysis. Given these complicating factors, we have made no attempt at this stage to perform an optimization to rigorously derive the best-fit exobase parameters. However, we note that in principle a sufficient set of measurements based on helium ion density ratios should provide enough information to constrain both the exobase density and temperature, without the same degree of colinearity intrinsic to some other methods utilized to investigate the structure of the Martian corona.

6 Implications and Conclusions

This manuscript provides a first study of the feasibility of utilizing helium ion measurements to probe the Martian hydrogen exosphere. We have shown with this work that singly ionized helium produced by charge exchange between solar wind alpha particles and neutral hydrogen exists and has a measurable signature in the region upstream from Mars. The observed solar wind speed dependence and spatial structure of this signal confirms the interpretation of its origin, and the seasonal variability thereby inferred for the hydrogen exosphere agrees well with extrapolations from a variety of other techniques. These measurements should ultimately help us refine our understanding of the role of the Martian seasonal cycle in the overall escape of hydrogen from Mars (Jakosky et al., 2018).

Utilizing solar wind helium to probe the Martian exosphere has both advantages and disadvantages over previously utilized methods. Given the rather small ion densities in question, the helium ion measurement provides only a weak signal, requiring integration over long time ranges to accumulate sufficient counts to isolate the trends of interest. Furthermore, isolating the helium ion signal requires the subtraction of a number of backgrounds of both instrumental and geophysical origin, some more well understood than others. On the other hand, the helium ion measurement has the advantage of providing a signal that is relatively straightforward to invert to derive a column density estimate. Given a sufficient number of such measurements, one could in principle determine the 3-d structure of the hydrogen corona and compare to exospheric models to extract parameters such as exobase density and temperature, as well as the presence of any non-thermal components. Furthermore, one can make these measurements anywhere in the magnetosheath or upstream region, allowing nearly continuous coverage of the Martian seasonal cycle and thus enabling detailed study of the interannual variability of the Martian exosphere.

Future studies could progress beyond this one by utilizing more sophisticated modeling of the trajectories of solar wind ions through the magnetosheath, thereby enabling a more direct comparison between data obtained in the sheath and the column densities predicted by parameterized exospheric models. One could also more explicitly account for other sources of singly ionized helium in the Martian environment, including pickup of neutral helium of both interstellar and Martian origin, and solar wind charge exchange with other neutrals. Accounting

for these sources would allow a better isolation of the signal from solar wind charge exchange with the hydrogen exosphere, and would also enable detailed characterization of the spatial structure and temporal variability of both interstellar and Martian helium.

Acknowledgments, Samples, and Data

We acknowledge support for this work from the MAVEN contract.

All MAVEN data and ephemerides used in this study are available from the Planetary Data System (https://pds-ppi.igpp.ucla.edu/mission/MAVEN). Specifically, SWIA data are available at https://doi.org/10.17189/1414182 and STATIC data are available at https://pds-ppi.igpp.ucla.edu/mission/MAVEN/MAVEN/STATIC. The helium ion density ratios computed from STATIC data and shown in the figures in the paper are archived at https://doi.org/10.5281/zenodo.5290791 (J. S. Halekas, 2021).

References

Aellig, M. R., Lazarus, A. J., & Steinberg, J. T. (2001). The solar wind helium abundance: Variation with wind speed and the solar cycle. *AIP Conference Proceedings*, *598*(1), 89–94. https://doi.org/10.1063/1.1433984

Bame, S. J., Hundhausen, A. J., Asbridge, J. R., & Strong, I. B. (1968). Solar Wind Ion Composition. *Physical Review Letters*, *20*(8), 393–395. https://doi.org/10.1103/PhysRevLett.20.393

Barabash, S., Kallio, E., Lundin, R., & Koskinen, H. (1995). Measurements of the nonthermal helium escape from Mars. *Journal of Geophysical Research: Space Physics*, *100*(A11), 21307–21316. https://doi.org/10.1029/95JA01914

Barnett, C. F., Hunter, H. T., Fitzpatrick, M. I., Alvarez, I., Cisneros, C., & Phaneuf, R. A. (1990). Atomic data for fusion. Volume 1: Collisions of H, H2, He and Li atoms and ions with atoms and molecules. *NASA STI/Recon Technical Report N*, *91*, 13238.

Bertucci, C., Romanelli, N., Chaufray, J. Y., Gomez, D., Mazelle, C., Delva, M., et al. (2013). Temporal variability of waves at the proton cyclotron frequency upstream from Mars: Implications for Mars distant hydrogen exosphere. *Geophysical Research Letters*, *40*(15), 3809–3813. https://doi.org/10.1002/grl.50709

Bhattacharyya, D., Clarke, J. T., Bertaux, J.-L., Chaufray, J.-Y., & Mayyasi, M. (2015). A strong seasonal dependence in the Martian hydrogen exosphere. *Geophysical Research Letters*, *42*(20), 8678–8685. https://doi.org/10.1002/2015GL065804

Burch, J. L., Cravens, T. E., Llera, K., Goldstein, R., Mokashi, P., Tzou, C.-Y., & Broiles, T. (2015). Charge exchange in cometary coma: Discovery of H− ions in the solar wind close to comet 67P/Churyumov-Gerasimenko. *Geophysical Research Letters*, *42*(13), 5125–5131. https://doi.org/10.1002/2015GL064504

Chaffin, M. S., Chaufray, J.-Y., Stewart, I., Montmessin, F., Schneider, N. M., & Bertaux, J.-L. (2014). Unexpected variability of Martian hydrogen escape. *Geophysical Research Letters*, *41*(2), 314–320. https://doi.org/10.1002/2013GL058578

Chaffin, M. S., Deighan, J., Schneider, N. M., & Stewart, A. I. F. (2017). Elevated atmospheric escape of atomic hydrogen from Mars induced by high-altitude water. *Nature Geoscience*, *10*(3), 174–178. https://doi.org/10.1038/ngeo2887

Chamberlain, J. W. (1963). Planetary coronae and atmospheric evaporation. *Planetary and Space Science*, *11*(8), 901–960. https://doi.org/10.1016/0032-0633(63)90122-3

Chanteur, G. M., Dubinin, E., Modolo, R., & Fraenz, M. (2009). Capture of solar wind alpha-particles by the Martian atmosphere. *Geophysical Research Letters*, *36*(23). https://doi.org/10.1029/2009GL040235

Clarke, J. T., Bertaux, J.-L., Chaufray, J.-Y., Gladstone, G. R., Quemerais, E., Wilson, J. K., & Bhattacharyya, D. (2014). A rapid decrease of the hydrogen corona of Mars. *Geophysical Research Letters*, *41*(22), 8013–8020. https://doi.org/10.1002/2014GL061803

Fedorova, A. A., Montmessin, F., Korablev, O., Luginin, M., Trokhimovskiy, A., Belyaev, D. A., et al. (2020). Stormy water on Mars: The distribution and saturation of atmospheric water during the dusty season. *Science*, *367*(6475), 297–300. https://doi.org/10.1126/science.aay9522

Fuselier, S. A., Shelley, E. G., Goldstein, B. E., Goldstein, R., Neugebauer, M., Ip, W.-H., et al. (1991). Observations of solar wind ion charge exchange in the Comet Halley coma. *The Astrophysical Journal*, *379*, 734. https://doi.org/10.1086/170549

Gloeckler, G., Möbius, E., Geiss, J., Bzowski, M., Chalov, S., Fahr, H., et al. (2004). Observations of the helium focusing cone with pickup ions. *Astronomy & Astrophysics*, *426*(3), 845–854. https://doi.org/10.1051/0004-6361:20035768

Gosling, J. T., Asbridge, J. R., Bame, S. J., Feldman, W. C., & Zwickl, R. D. (1980). Observations of large fluxes of He+ in the solar wind following an interplanetary shock. *Journal of Geophysical Research: Space Physics*, *85*(A7), 3431–3434. https://doi.org/10.1029/JA085iA07p03431

Halekas, J. S. (2017). Seasonal variability of the hydrogen exosphere of Mars. *Journal of Geophysical Research (Planets)*, *122*(5), 901–911. https://doi.org/10.1002/2017JE005306

Halekas, J. S. (2021). Helium Ion Density Ratios Upstream from Mars [Data set]. Zenodo. https://doi.org/10.5281/zenodo.5290791

Halekas, J. S., Taylor, E. R., Dalton, G., Johnson, G., Curtis, D. W., McFadden, J. P., et al. (2015). The Solar Wind Ion Analyzer for MAVEN. *Space Science Reviews*, *195*(1–4), 125–151. https://doi.org/10.1007/s11214-013-0029-z

Halekas, J. S., Ruhunusiri, S., Harada, Y., Collinson, G., Mitchell, D. L., Mazelle, C., et al. (2017). Structure, dynamics, and seasonal variability of the Mars-solar wind interaction: MAVEN Solar Wind Ion Analyzer in-flight performance and science results. *Journal of Geophysical Research (Space Physics)*, *122*(1), 547–578. https://doi.org/10.1002/2016JA023167

Halekas, J. S., Ruhunusiri, S., Vaisberg, O. L., Harada, Y., Espley, J. R., Mitchell, D. L., et al. (2020). Properties of Plasma Waves Observed Upstream From Mars. *Journal of Geophysical Research: Space Physics*, *125*(9), e2020JA028221. https://doi.org/10.1029/2020JA028221

Jakosky, B. M., Lin, R. P., Grebowsky, J. M., Luhmann, J. G., Mitchell, D. F., Beutelschies, G., et al. (2015). The Mars Atmosphere and Volatile Evolution (MAVEN) Mission. *Space Science Reviews*, *195*(1–4), 3–48. https://doi.org/10.1007/s11214-015-0139-x

Jakosky, B. M., Brain, D., Chaffin, M., Curry, S., Deighan, J., Grebowsky, J., et al. (2018). Loss of the Martian atmosphere to space: Present-day loss rates determined from MAVEN observations and integrated loss through time. *Icarus*, *315*, 146–157. https://doi.org/10.1016/j.icarus.2018.05.030

Kasper, J. C., Stevens, M. L., Lazarus, A. J., Steinberg, J. T., & Ogilvie, K. W. (2007). Solar Wind Helium Abundance as a Function of Speed and Heliographic Latitude: Variation through a Solar Cycle. *The Astrophysical Journal*, *660*(1), 901–910. https://doi.org/10.1086/510842

Krasnopolsky, V. A., Chakrabarti, S., & Gladstone, G. R. (1993). Helium in the Martian atmosphere. *Journal of Geophysical Research: Planets*, *98*(E8), 15061–15068. https://doi.org/10.1029/93JE00534

McFadden, J. P., Kortmann, O., Curtis, D., Dalton, G., Johnson, G., Abiad, R., et al. (2015). MAVEN SupraThermal and Thermal Ion Compostion (STATIC) Instrument. *Space Science Reviews*, *195*(1–4), 199–256. https://doi.org/10.1007/s11214-015-0175-6

Möbius, E., Hovestadt, D., Klecker, B., Scholer, M., Gloeckler, G., & Ipavich, F. M. (1985). Direct observation of He + pick-up ions of interstellar origin in the solar wind. *Nature*, *318*(6045), 426–429. https://doi.org/10.1038/318426a0

Ogilvie, K. W., & Coplan, M. A. (1995). Solar wind composition. *Reviews of Geophysics*, *33*(S1), 615–622. https://doi.org/10.1029/95RG00122

Rahmati, A., Larson, D. E., Cravens, T. E., Lillis, R. J., Halekas, J. S., McFadden, J. P., et al. (2018). Seasonal Variability of Neutral Escape from Mars as Derived From MAVEN Pickup Ion Observations. *Journal of Geophysical Research (Planets)*, *123*(5), 1192–1202. https://doi.org/10.1029/2018JE005560

Romanelli, N., Mazelle, C., Chaufray, J. Y., Meziane, K., Shan, L., Ruhunusiri, S., et al. (2016). Proton cyclotron waves occurrence rate upstream from Mars observed by MAVEN: Associated variability of the Martian upper atmosphere. *Journal of Geophysical Research (Space Physics)*, *121*(11), 11,113-11,128. https://doi.org/10.1002/2016JA023270

Romeo, O. M., Romanelli, N., Espley, J. R., Mazelle, C., DiBraccio, G. A., Gruesbeck, J. R., & Halekas, J. S. (2021). Variability of Upstream Proton Cyclotron Wave Properties and Occurrence at Mars Observed by MAVEN. *Journal of Geophysical Research: Space Physics*, *126*(2), e2020JA028616. https://doi.org/10.1029/2020JA028616

Schwenn, R., Rosenbauer, H., & Mühlhäuser, K.-H. (1980). Singly-ionized helium in the driver gas of an interplanetary shock wave. *Geophysical Research Letters*, *7*(3), 201–204. https://doi.org/10.1029/GL007i003p00201

Shelley, E. G., Fuselier, S. A., Balsiger, H., Drake, J. F., Geiss, J., Goldstein, B. E., et al. (1987). Charge Exchange of Solar Wind Ions in the Coma of Comet p/ Halley. *Astronomy and Astrophysics*, *187*, 304.

Stenberg, G., Nilsson, H., Futaana, Y., Barabash, S., Fedorov, A., & Brain, D. (2011). Observational evidence of alpha-particle capture at Mars. *Geophysical Research Letters*, *38*(9). https://doi.org/10.1029/2011GL047155

Stone, S. W., Yelle, R. V., Benna, M., Lo, D. Y., Elrod, M. K., & Mahaffy, P. R. (2020). Hydrogen escape from Mars is driven by seasonal and dust storm transport of water. *Science*, *370*(6518), 824–831. https://doi.org/10.1126/science.aba5229

514 Trotignon, J. G., Mazelle, C., Bertucci, C., & Acuña, M. H. (2006). Martian shock and magnetic pile-up boundary
515 positions and shapes determined from the Phobos 2 and Mars Global Surveyor data sets. *Planetary and*
516 *Space Science*, *54*(4), 357–369. https://doi.org/10.1016/j.pss.2006.01.003
517 Wedlund, C. S., Kallio, E., Alho, M., Nilsson, H., Wieser, G. S., Gunell, H., et al. (2016). The atmosphere of comet
518 67P/Churyumov-Gerasimenko diagnosed by charge-exchanged solar wind alpha particles. *Astronomy &*
519 *Astrophysics*, *587*, A154. https://doi.org/10.1051/0004-6361/201527532
520 Yamauchi, M., Hara, T., Lundin, R., Dubinin, E., Fedorov, A., Sauvaud, J.-A., et al. (2015). Seasonal variation of
521 Martian pick-up ions: Evidence of breathing exosphere. *Planetary and Space Science*, *119*, 54–61.
522 https://doi.org/10.1016/j.pss.2015.09.013
523